

Directed flow in relativistic heavy-ion collisions from a multiphase transport model

Chong-Qiang Guo,^{1,2} Chun-Jian Zhang,^{1,2} and Jun Xu^{*1}

¹Shanghai Institute of Applied Physics, Chinese Academy of Sciences, Shanghai 201800, China

²University of Chinese Academy of Sciences, Beijing 100049, China

(Dated: December 3, 2024)

We have studied the directed flow in $^{197}\text{Au}+^{197}\text{Au}$ collisions at $\sqrt{s_{NN}} = 200$ and 39 GeV within a multiphase transport model. As the partonic phase evolves with time, the slope of the parton directed flow at mid-rapidity region changes from negative to positive as a result of the later dynamics at 200 GeV, while it remains negative at 39 GeV due to the shorter life time of the partonic phase. The directed flow splitting for various quark species due to their different initial eccentricities is observed at 39 GeV, while the splitting is very small at 200 GeV. Effects of the hadronization and the hadronic rescatterings on the directed flow are further discussed. Our study serves as a baseline on the understanding of the directed flow in the absence of the mean-field potentials and other exotic mechanisms.

PACS numbers: 25.75.-q, 25.75.Ld, 24.10.Lx

I. INTRODUCTION

The main purpose of relativistic heavy-ion collision experiments is to study the properties of the quark-gluon plasma (QGP) [1–4] and to understand the hadron-quark phase transition. The anisotropic flow, defined as $v_n = \langle \cos[n(\phi - \Psi_n)] \rangle$ with ϕ being the particle azimuthal angle in momentum space with respect to the event plane Ψ_n and $\langle \dots \rangle$ denoting the event average, is an important observable in characterizing how the anisotropy in the initial coordinate space develops into that in the final momentum space, as a result of the strong interaction in the QGP matter created in relativistic heavy-ion collisions. The first-order anisotropic flow is named as the directed flow (v_1) (see Ref. [5] for a recent review), and it contains the rapidity-odd component and the rapidity-even component. The rapidity-odd component $v_1^{odd}(y) = -v_1^{odd}(-y)$, which is traditionally called the sideward flow, is attributed to the collective sideways deflection of particles. The rapidity-even component $v_1^{even}(y) = v_1^{even}(-y)$ was realized recently [6, 7], and it is attributed to the event-by-event fluctuation in the initial state of the colliding nuclei. In the present study we only talk about the rapidity-odd component of the directed flow.

Both hydrodynamic [8] and transport model [9] studies have shown that $v_1(y)$ in the midrapidity region, especially that for baryons, is sensitive to the equation of state (EoS) of the produced matter. With the increasing collision energies, these calculations predict that the slope of v_1 for charged particles near mid-rapidity region changes from positive to negative, which is named in the literature as the "antiflow" [10], the "third flow component" [11], or the "wobble" [12]. It is argued that this phenomenon could be a possible signature of the phase transition, originating from the softness of the EoS in the

hadron-quark mixed phase. On the other hand, the effects of the EoS could be understood only if the directed flow from the cascade scenario without mean-field potentials is well settled. In addition, the effect of hadronization on the directed flow has not attracted much attention yet.

Recently, RHIC-STAR Collaboration have reported the directed flow of protons and pions in the beam-energy-scan program [13]. It has been found that the slope of the net-proton directed flow changes sign twice between $\sqrt{s_{NN}} = 11.5$ GeV and 39 GeV, and has a minimum between $\sqrt{s_{NN}} = 11.5$ GeV and 19.6 GeV. Besides, splittings of the directed flow between protons and antiprotons as well as that between π^+ and π^- were observed at lower collision energies but become small at higher collision energies. Efforts have been made using transport model calculations [14–16] but none of them have described the experimental data of the directed flow at various collision energies very satisfactorily so far.

In this study we investigate the directed flow in relativistic heavy-ion collisions within a multiphase transport (AMPT) model [17]. Different from the previous study [18], we will study the time evolution of the directed flow in the partonic phase, the splitting of the directed flow between different quark species, and the effect due to hadronization. This study is carried out based on the original AMPT model with only scatterings between particles. This serves as a baseline of the directed flow properties that one needs to understand before incorporating the EoS or the mean-field potential. The rest of the paper is organized as follows. Section II provides a brief introduction of the AMPT model. The detailed analysis and discussions of the directed flow results are given in Sec. III. Finally, a summary and outlook is given in Sec. IV.

*Corresponding author: xujun@sinap.ac.cn

II. THE AMPT MODEL

The string melting version of the AMPT model [17], which is used in the present study, mainly consists of four parts: the initial condition generated by Heavy Ion Jet Interaction Generator (HIJING) model [19], the partonic evolution described by Zhang's parton cascade (ZPC) model [20], a coalescence model to describe the hadronization process, and the hadronic evolution described by a relativistic transport (ART) model [21]. The HIJING model generates hadrons with proton-proton scatterings as the building brick together with the nuclear shadowing effect and the Glauber geometry for the colliding nuclei at relativistic energies. The initial phase-space distribution of quarks is generated by melting hadrons produced in HIJING, containing reasonable event-by-event fluctuations. The quark interaction in the ZPC model is described by the partonic two-body elastic scatterings with the differential cross section given by

$$\frac{d\sigma}{dt} \approx \frac{9\pi\alpha_s^2}{2(t - \mu^2)^2}, \quad (1)$$

where t is the standard Mandelstam variable for four-momentum transfer. In the present study we set the strong coupling constant α_s to be 0.47 and the parton screening mass μ to be 3.2264 fm^{-1} , leading to the total cross section of 3 mb. The evolution of the partonic phase ends when the distance between quarks is out of the radius of the cross section. The hadronization is described by a spatial coalescence model which allows a pair of nearest quark and antiquark to form a meson and three nearest quarks or antiquarks to form a baryon or an antibaryon, with the mass and species of the hadron determined by the invariant mass and the flavors of these constituent partons. In the AMPT version used in the present study, hadrons are formed from nearest quark in coordinate space, while whether they are close in momentum space is not guaranteed. In addition, meson coalescence is proceeded before baryon coalescence in the AMPT version used in the present study, which reduces the combinations of three quarks that are close in coordinate space and makes the baryon coalescence less realistic. An improvement can be done with mix-event coalescence [22] in the future. In order to see the effect of a more realistic coalescence on the directed flow, we have also checked with the dynamical coalescence [23] based on the Wigner function calculation which will be detailed in Sec. IIIB and APPENDIX A. The spatial coalescence in the AMPT model is followed by the ART model that contains various elastic, inelastic, and decay channels to describe the hadronic evolution.

III. ANALYSIS AND RESULTS

In the present study, we employ the AMPT model to investigate the directed flow in mid-central ($b = 5 \text{ fm}$)

$^{197}\text{Au}+^{197}\text{Au}$ collisions at $\sqrt{s_{NN}} = 200$ and 39 GeV, corresponding to the top RHIC energy and a typical energy in the beam-energy-scan program. Typically, we focus on the time evolution of v_1 , the splitting of v_1 for various particle species, and the hadronization effect on v_1 . The directed flow is calculated with respect to the theoretical reaction plane, i.e., $v_1 = \langle \cos(\phi) \rangle$, in the present study.

A. Time evolution of v_1 in the partonic phase

Before we investigate the time evolution of v_1 , let's first have a global impression on the density evolution in the partonic phase. The density contours at time 0.5, 1, 1.5, 2, 4, 6, 8, and 10 fm/c in the x - z plane, i.e., the reaction plane with x the direction of the impact parameter and z the beam direction, in mid-central Au+Au collisions at $\sqrt{s_{NN}} = 200$ GeV and 39 GeV are displayed in Figs. 1 and 2, respectively. We found that a large amount of partons are formed before 0.5 fm/c. The strong interaction between partons lasts until 4 or 6 fm/c. After that the interaction becomes weaker, and the disk-like partonic matter moves away in the $\pm z$ direction. The density evolutions are similar at $\sqrt{s_{NN}} = 200$ GeV and 39 GeV, although a higher quark density is observed at higher collision energies where the life time of the partonic phase is expected to last longer. The direction of $x \cdot z > 0$ ($x \cdot z < 0$) is intuitively labelled as the "+" ("−") direction for the ease of discussion, corresponding to the positive flow and the antiproflow. The relative numbers of particles moving in the "+" and the "−" directions determine the net directed flow.

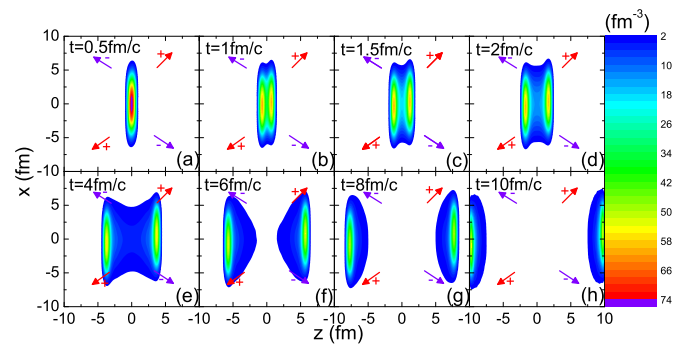


FIG. 1: (Color online) Density contours in the x - z plane at different time steps in the partonic phase of Au + Au collisions at $\sqrt{s_{NN}} = 200$ GeV and impact parameter $b = 5 \text{ fm}$, with different colors indicating the quark number densities. The particles that move in the "+" ("−") direction contribute to the positive flow (antiproflow).

The directed flow of quarks in mid-central Au+Au collisions at $\sqrt{s_{NN}} = 200$ GeV and 39 GeV at different time steps is displayed in Fig. 3, with the solid lines from a cubic fit of $v_1(y) = F_1 y + F_3 y^3$. The initial v_1 at both collision energies are very small as expected. As the system evolves, the slope of the directed flow at $\sqrt{s_{NN}} =$

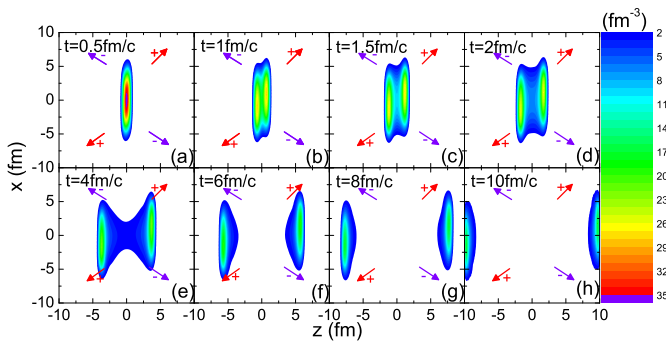


FIG. 2: (Color online) Same as Fig. 1 but for Au + Au collisions at $\sqrt{s_{NN}} = 39$ GeV.

200 GeV grows to a maximum negative value at around 4 fm/c and then gradually becomes positive, while that at $\sqrt{s_{NN}} = 39$ GeV grows to a maximum negative value at around 6 fm/c and becomes saturated. The maximum slope is larger at 39 GeV than at 200 GeV. On the other hand, the strong scatterings among partons mostly end around 4 \sim 6 fm/c, and the interaction is expected to become weaker in the later dynamics, according to the density evolution shown in Figs. 1 and 2. However, it is seen that the later dynamics reverses the slope of the directed flow at $\sqrt{s_{NN}} = 200$ GeV but is unable to reverse that at $\sqrt{s_{NN}} = 39$ GeV, due to the shorted life time of the partonic phase at lower collision energies. We note that a similar non-monotonic behavior of the directed flow was observed in Ref. [14] but not discussed in detail.

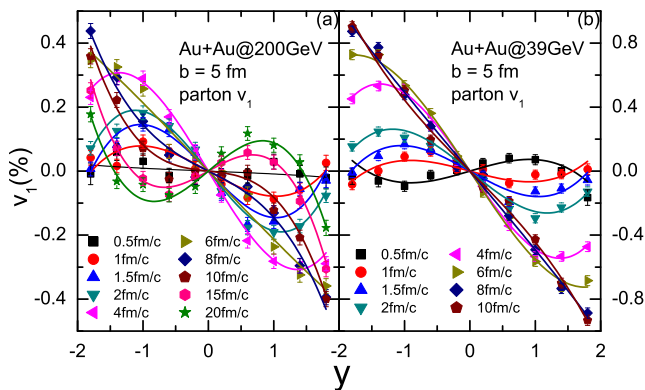


FIG. 3: (Color online) Directed flow (v_1) of quarks versus rapidity (y) at different time steps in mid-central Au+Au collisions at $\sqrt{s_{NN}} = 200$ GeV (a) and 39 GeV (b).

B. Saturation of v_1

Next, we display the integrated directed flow at forward and backward rapidities as a function of time in Fig. 4. It is interesting to see that the integrated v_1 at the forward (backward) rapidity monotonically becomes

more negative (positive) as the system evolves, although the directed flow at different rapidity regions changes in a complicated manner as shown in Fig. 3. At $\sqrt{s_{NN}} = 200$ GeV the integrated directed flow becomes saturated at about 8 fm/c, while at $\sqrt{s_{NN}} = 39$ GeV it is saturated at a later time. In addition, the magnitude of the integrated v_1 is larger at lower collision energies due to the larger initial first-order eccentricity, as will be discussed in Fig. 7.

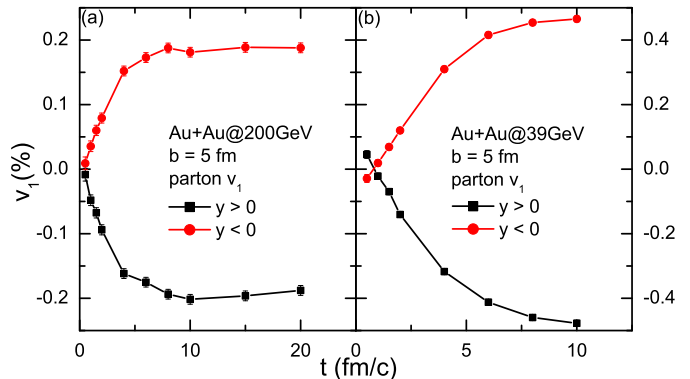


FIG. 4: (Color online) The time evolution of quark directed flow (v_1) at forward and backward rapidities in mid-central Au+Au collisions at $\sqrt{s_{NN}} = 200$ GeV (a) and 39 GeV (b).

In order to understand the time evolution of the v_1 slope in Fig. 3 with saturated integrated directed flow as shown in Fig. 4, we plot the time evolution of $d(N_+ - N_-)/dy$ as a function of rapidity y in Fig. 5, with N_+ (N_-) being the number of particles that contribute positively (negatively) to v_1 at forward rapidity but negatively (positively) to v_1 at backward rapidity, corresponding to the number of particles moving in the “+(-)” direction as labelled in Figs. 1 and 2, contributing to the positive flow (antiflow). It is seen in Fig. 5 that N_+ is almost equal to N_- at the initial stage, corresponding to a zero v_1 . As the system evolves, two negative peaks grow at forward and backward rapidities, corresponding to the picture that more particles move to $-x$ direction at forward rapidity and to $+x$ direction at backward rapidities, i.e., a net antiflow. As these particles are further accelerated in the later dynamics after 4 \sim 6 fm/c in the beam direction, the peaks gradually move to larger rapidity regions. At the later stage of the partonic phase at $\sqrt{s_{NN}} = 200$ GeV, only particles that contribute to the positive flow stay in the mid-rapidity region, leading to a positive slope of mid-rapidity v_1 . So, the time evolution of the v_1 slope in Fig. 3 at $\sqrt{s_{NN}} = 200$ GeV is due to the transfer of particles among different rapidity regions, leading to a positive v_1 slope at the freeze-out stage. At $\sqrt{s_{NN}} = 39$ GeV, the saturation of v_1 takes longer time while the life time of the partonic phase is shorter, leading to a negative v_1 slope at the freeze-out stage.

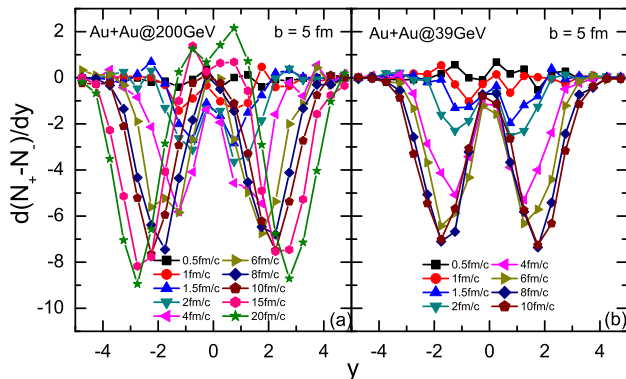


FIG. 5: (Color online) Rapidity dependence of $d(N_+ - N_-)/dy$ indicating the competition between the positive flow and the antiflow at different time steps in partonic phase of mid-central Au+Au collisions at $\sqrt{s_{NN}} = 200$ GeV (a) and 39 GeV (b).

C. Splitting of v_1 for various quark species

The results discussed in the previous subsections are the average over all quark species. Due to the finite chemical potentials reached at lower collision energies, it is always observed that there are splittings of quantities between particles and antiparticles as well as those between particles of different isospin states. The typical examples are splittings of the elliptic flow [24] and the directed flow [13] between protons and antiprotons as well as those between π^+ and π^- . Based on the AMPT model with only particle cascade, we will see how large the splitting of directed flow between various quark species is, in the absence of the mean-field potential as well as other exotic mechanisms.

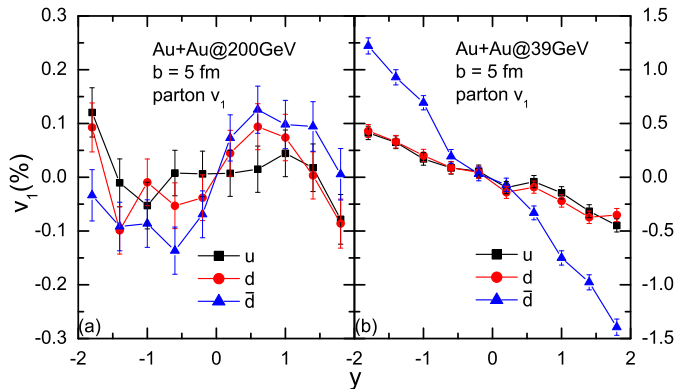


FIG. 6: (Color online) Final directed flow (v_1) of u , d , and \bar{d} quarks versus rapidity (y) in mid-central Au+Au collisions at $\sqrt{s_{NN}} = 200$ GeV (a) and 39 GeV (b).

Figure 6 displays the directed flow of u , d , and \bar{d} quarks at their freeze-out stage in mid-central Au+Au collisions at $\sqrt{s_{NN}} = 200$ GeV and 39 GeV. At $\sqrt{s_{NN}} = 200$ GeV the v_1 splitting between quarks and antiquarks as well

as that between u and d quarks are already seen but the difference is comparable to the statistical error, while at $\sqrt{s_{NN}} = 39$ GeV it is clearly seen that \bar{d} quarks have a more negative directed flow than u and d quarks. The splitting between directed flows of various quark species could be partially responsible for the v_1 splitting between protons and antiprotons as well as that between π^+ and π^- , as reported in Ref. [13].

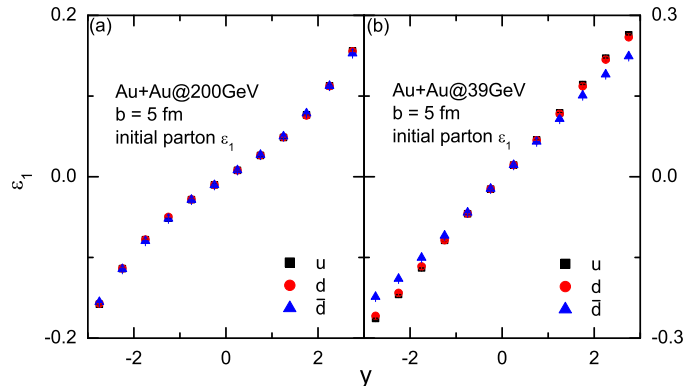


FIG. 7: (Color online) Initial first-order eccentricity (ϵ_1) of u , d , and \bar{d} quarks versus rapidity (y) in mid-central Au+Au collisions at $\sqrt{s_{NN}} = 200$ GeV (a) and 39 GeV (b).

The mechanism how the initial eccentricity (ϵ_n) develops into the final elliptic flow (v_2) and triangular flow (v_3) has been extensively studied (see, e.g., Refs. [25–27]). Generally, a larger initial eccentricity leads to a larger final anisotropic flow. Since the rapidity-odd directed flow in the present study is calculated with respect to the theoretical reaction plane, we calculate the correspondingly ϵ_1 according to the particle azimuthal angle ϕ_s in coordinate space as

$$\epsilon_1 = \langle \cos(\phi_s) \rangle, \quad (2)$$

with $\langle \dots \rangle$ denoting the event average. Figure 7 shows the rapidity distribution of the initial first-order eccentricity for various quark species at both $\sqrt{s_{NN}} = 200$ GeV and 39 GeV. It is seen that ϵ_1 has a positive slope with respect to the rapidity. Due to the larger inelastic proton-proton scattering cross section at higher collision energies used in HIJING [19], the effective overlap region is slightly larger at $\sqrt{s_{NN}} = 200$ GeV compared to that at 39 GeV, leading to a slightly smaller centrality at higher collision energies even with the same impact parameter $b = 5$ fm. This leads to a larger slope of ϵ_1 at lower collision energies compared with that at higher collision energies, which is responsible for the larger maximum v_1 slope at about $4 \sim 6$ fm/c in Fig. 3 and a larger saturated v_1 in Fig. 4 at lower collision energies. Moreover, it is seen that at $\sqrt{s_{NN}} = 200$ GeV the initial ϵ_1 is similar for all the quark species, while at $\sqrt{s_{NN}} = 39$ GeV \bar{d} quarks have a smaller slope of ϵ_1 with respect to the rapidity. Since these quarks are melted from hadrons produced in HIJING, the difference is attributed to the different

production mechanisms of hadrons that have different baryon or isospin charges. This explains the different \bar{d} directed flow compared to v_1 of other quark species. The ϵ_1 for u and d quarks is the same at higher collision energies, and the difference is barely able to observe at lower collision energies.

D. Effect of hadronization on v_1

The directed flow of freeze-out quarks discussed in the previous subsections will be modified in the hadronization process. In the present study we investigate the hadronization from a dynamical coalescence model [23, 28] and the default spatial coalescence model as in AMPT. In the dynamical coalescence model, the probability to form a hadron is proportional to the quark Wigner function of that hadron, and the proportional coefficient is the statistical factor by considering the spin, flavor, and color degrees of freedom. For detailed formulae we refer the reader to APPENDIX A. In the dynamical coalescence model, partons that are close in phase space have a larger probability to form hadrons, while in the default spatial coalescence model in AMPT, hadrons are formed by nearest combinations of partons in coordinate space as discussed in Sec. II, and all the partons are force to be used up after hadronization. To speed up the program, in the dynamical coalescence only the parton combinations with the relative momentum $\delta\mathbf{p} \leq 2.5$ GeV/c are allowed to form hadrons, since the probability for combinations with larger relative momenta to form hadrons is rather small.

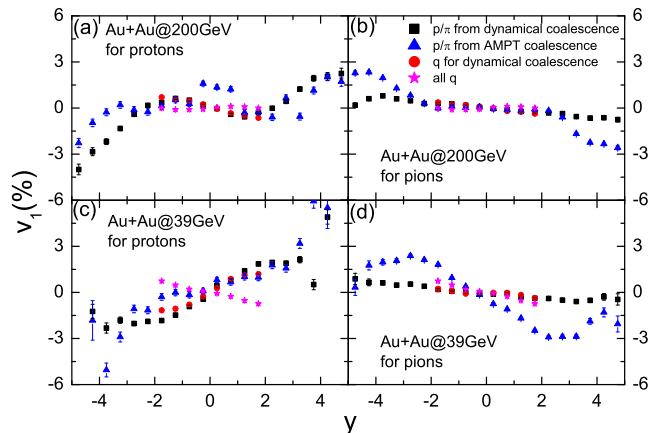


FIG. 8: (Color online) Directed flow (v_1) of protons and charged pions from the dynamical coalescence and from the default spatial coalescence in the AMPT model, as well as v_1 of their constituent quarks weighted by the Wigner function, and v_1 of all quarks at their freeze-out stage as a function of rapidity in mid-central Au+Au collisions at $\sqrt{s_{NN}} = 200$ GeV [(a) and (b)] and 39 GeV [(c) and (d)]. See text for details.

Figure 8 displays the directed flow of protons and charged pions from the dynamical coalescence and from

the spatial coalescence in AMPT, as well as that of their constituent quarks weighted by the Wigner function, and that of all quarks at their freeze-out stage. The difference between v_1 from the dynamical coalescence and that from the default spatial coalescence in AMPT is observed, consistent with the statement in Ref. [14] that the directed flow is sensitive to the hadronization treatment. On the other hand, the spatial coalescence in AMPT needs further improvement [22], especially for baryons as mentioned in Sec. II. It is interesting to see that the directed flow of constituent quarks weighted by the Wigner function is quite different from that of all quarks at their freeze-out stage. This means that in the dynamical coalescence scenario only part of partons close in phase space dominate the contribution of forming hadrons, while their directed flow is quite different from the rest partons. The deep reason for this is worth further investigation. As a consequence, the directed flow of formed protons or pions is similar to that of their constituent partons but different from that of the overall partons. The difference is larger for baryons than for mesons, and the v_1 slope of protons from the dynamical coalescence has even changed its sign compared with that of the overall partons.

E. Effect of hadronic evolution on v_1

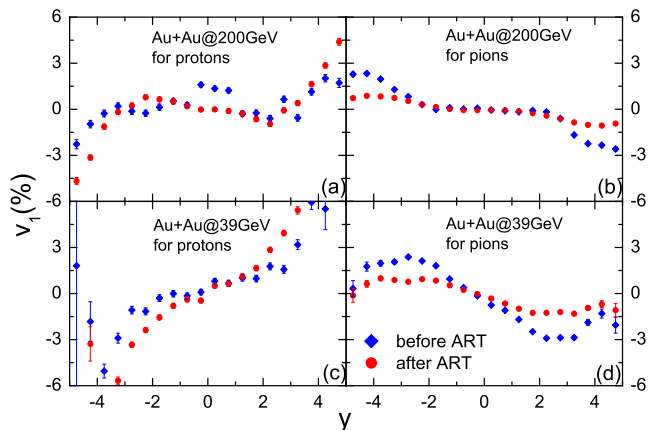


FIG. 9: (Color online) Directed flow (v_1) of protons and charged pions versus rapidity (y) before and after hadronic rescatterings in mid-central Au+Au collisions at $\sqrt{s_{NN}} = 200$ GeV [(a) and (b)] and 39 GeV [(c) and (d)].

The directed flow of hadrons after hadronization presented in the previous subsection is further modified by the hadronic evolution described by ART, containing various elastic, inelastic, and decay channels. To illustrate the effect of hadronic rescatterings on v_1 in the AMPT model, we present in Fig. 9 the directed flow of initial (before ART) and final (after ART) protons and charged pions in mid-central Au+Au collision at $\sqrt{s_{NN}} = 200$ GeV and 39 GeV. After hadronic scatterings, it is seen

that the slope of the directed flow generally becomes less negative or increases, while the sign of the v_1 slope near mid-rapidity region is not changed. The effect of the hadronic evolution on v_1 is seen to be larger at lower collision energies compared to that at higher collision energies.

IV. SUMMARY AND OUTLOOK

To summarize, we have studied in detail the effects of partonic scatterings, hadronization, and hadronic rescatterings on the directed flow in relativistic heavy-ion collisions within the framework of a multiphase transport model. Due to the larger proton-proton inelastic scattering cross section in HIJING at higher collision energies, which leads to a larger overlap and a smaller initial first-order eccentricity at higher collision energies, the directed flow is saturated at a smaller value at $\sqrt{s_{NN}} = 200$ GeV compared to that at 39 GeV. As the system evolves, a non-monotonic behavior of the directed flow is observed at higher collision energies, and the later dynamics is able to change the slope sign of the directed flow at mid-rapidity region, as a result of the longer life time of the partonic phase, but this is not observed at lower collision energies. The splitting of the directed flow for various quark species is observed at lower collision energies due to their different initial eccentricities, while such splitting becomes very small at higher collision energies. The directed flow is further affected by the hadronization and the hadronic rescatterings.

In the future study, we will improve the coalescence and introduce the mean-field potential to the multiphase transport model as in Ref. [22, 29]. It will be of great interest to study quantitatively how the results obtained in this work are modified by the mean-field potentials, which are expected to be different for different quark and hadron species. On the other hand, it is interesting to see that the directed flow of hadrons is mainly determined by only part of partons that are close in phase space based on the dynamical coalescence. It is worthy to investigate in more detail the feature of these partons and have a deeper understanding of the relation between the anisotropic flow and the hadron-quark phase transition.

Acknowledgments

We thank Chen Zhong for maintaining the high-quality performance of the computer facility. This work was supported by the Major State Basic Research Development Program (973 Program) of China under Contract Nos. 2015CB856904 and 2014CB845401, the National Natural Science Foundation of China under Grant Nos. 11475243 and 11421505, the "100-talent plan" of Shanghai Institute of Applied Physics under Grant Nos. Y290061011 and Y526011011 from the Chinese Academy of Sciences, the Shanghai Key Laboratory of Particle Physics and Cosmology under Grant No. 15DZ2272100, and the "Shanghai Pujiang Program" under Grant No. 13PJ1410600.

APPENDIX A. DYNAMICAL COALESCENCE FOR HADRONS WITH WIGNER FUNCTION

In the dynamical coalescence model, the probability for a pair of quark and antiquark to form a meson is proportional to the quark Wigner function of the meson times the statistical factor, i.e.,

$$f_M(\boldsymbol{\rho}, \mathbf{k}_\rho) = 8g_M \exp\left(-\frac{\boldsymbol{\rho}^2}{\sigma_\rho^2} - \mathbf{k}_\rho^2 \sigma_\rho^2\right), \quad (\text{A.3})$$

where $g_M = 1/36$ is the statistical factor for pions, and

$$\boldsymbol{\rho} = \frac{1}{\sqrt{2}}(\mathbf{r}_1 - \mathbf{r}_2), \quad (\text{A.4})$$

$$\mathbf{k}_\rho = \sqrt{2} \frac{m_2 \mathbf{k}_1 - m_1 \mathbf{k}_2}{m_1 + m_2} \quad (\text{A.5})$$

are the relative distance in the coordinate and momentum space for the two-particle system, with m_i , \mathbf{r}_i , and \mathbf{k}_i being the mass, coordinate, and momentum of the i th particle, respectively. The width parameter σ_ρ is related to the root-mean-square (RMS) radius of the meson through the relation

$$\langle r_M^2 \rangle = \frac{3}{2} \frac{m_1^2 + m_2^2}{(m_1 + m_2)^2} \sigma_\rho^2. \quad (\text{A.6})$$

Similarly, the probability for three light quarks to form a baryon is expressed as

$$f_B(\boldsymbol{\rho}, \boldsymbol{\lambda}, \mathbf{k}_\rho, \mathbf{k}_\lambda) = 8^2 g_B \exp\left(-\frac{\boldsymbol{\rho}^2}{\sigma_\rho^2} - \frac{\boldsymbol{\lambda}^2}{\sigma_\lambda^2} - \mathbf{k}_\rho^2 \sigma_\rho^2 - \mathbf{k}_\lambda^2 \sigma_\lambda^2\right), \quad (\text{A.7})$$

where $g_B = 1/108$ is the statistical factor for protons, and

$$\boldsymbol{\lambda} = \sqrt{\frac{2}{3}} \left(\frac{m_1 \mathbf{r}_1 + m_2 \mathbf{r}_2}{m_1 + m_2} - \mathbf{r}_3 \right), \quad (\text{A.8})$$

$$\mathbf{k}_\lambda = \sqrt{\frac{3}{2}} \frac{m_3(\mathbf{k}_1 + \mathbf{k}_2) - (m_1 + m_2)\mathbf{k}_3}{m_1 + m_2 + m_3} \quad (\text{A.9})$$

are the relative distance in the coordinate and momentum space between the third particle and the system formed by the first and the second particle. The width parameter σ_λ is related to the RMS radius of the baryon through the relation

$$\begin{aligned} \langle r_B^2 \rangle &= \frac{3}{4} \frac{(m_1 + m_2)}{m_1 m_2 (m_1 + m_2 + m_3)^2} \sigma_\lambda^2 \\ &\times [m_2 m_3 (m_2 + m_3) + m_1 m_3 (m_1 + m_3) \\ &+ m_1 m_2 (m_1 + m_2)]. \end{aligned} \quad (\text{A.10})$$

The RMS radius of the produced hadron is taken from Ref. [30], which is 0.61 fm for π^+ and 0.877 fm for protons, respectively.

-
- [1] I. Arsene *et al.* (PHOBOS Collaboration), Nucl. Phys. **A757**, 1 (2005).
- [2] B. B. Back *et al.* (BRAHMS Collaboration), Nucl. Phys. **A757**, 28 (2005).
- [3] J. Adams *et al.* (STAR Collaboration), Nucl. Phys. **A757**, 102 (2005).
- [4] K. Adcox *et al.* (PHENIX Collaboration), Nucl. Phys. **A757**, 184 (2005).
- [5] S. Singha *et al.*, Advances in High Energy Physics **16**, 2836989 (2016).
- [6] D. Teaney and L. Yan, Phys. Rev. C **83**, 064904 (2011).
- [7] M. Luzum and J. Y. Ollitrault, Phys. Rev. Lett. **106**, 102301 (2011).
- [8] H. Stöcker, Nucl. Phys. A **750**, 121 (2005).
- [9] S. A. Bass *et al.*, Prog. Part. Nucl. Phys. **41**, 255 (1998).
- [10] J. Brachmann *et al.*, Phys. Rev. C **61**, 024909 (2000).
- [11] L. P. Csernai and D. Röhrich, Phys. Lett. B **458**, 454 (1999).
- [12] R. J. M. Snellings, H. Sorge, S. A. Voloshin, F. Q. Wang, and N. Xu, Phys. Rev. Lett. **84**, 2803 (2000).
- [13] L. Adamczyk *et al.* (STAR Collaboration), Phys. Rev. Lett. **112**, 162301 (2014).
- [14] J. Steinheimer *et al.*, Phys. Rev. C **89**, 054913 (2014).
- [15] V. P. Konchakovski *et al.*, Phys. Rev. C **90**, 014903 (2014).
- [16] Y. Nara *et al.*, Phys. Rev. C **94**, 034906 (2016).
- [17] Z. W. Lin, C. M. Ko, B. A. Li, B. Zhang, and S. Pal, Phys. Rev. C **72**, 064901 (2005).
- [18] J. Y. Chen, J. X. Zuo, X. Z. Cai, F. Liu, Y. G. Ma, and A. H. Tang, Phys. Rev. C **81**, 014904 (2010).
- [19] X. N. Wang and M. Gyulassy, Phys. Rev. D **44**, 3501 (1991).
- [20] B. Zhang, Comput. Phys. Commun. **109**, 193 (1998).
- [21] B. A. Li and C. M. Ko, Phys. Rev. C **52**, 2037 (1995).
- [22] J. Xu and C. M. Ko, Phys. Rev. C **94**, 054909 (2016).
- [23] V. Greco, C. M. Ko, and P. Levai, Phys. Rev. Lett. **90**, 202302 (2003); Phys. Rev. C **68**, 034904 (2003).
- [24] L. Adamczyk *et al.* (STAR Collaboration), Phys. Rev. Lett. **110**, 142301 (2013).
- [25] B. Alver and G. Roland, Phys. Rev. C **81**, 054905 (2010).
- [26] Roy A. Lacey *et al.*, Phys. Rev. C **83**, 044902 (2011).
- [27] H. Petersen, G. Y. Qin, S. A. Bass, and B. Müller, Phys. Rev. C **82**, 041901(R) (2010).
- [28] C. M. Ko, T. Song, F. Li, V. Greco, and S. Plumari, Nucl. Phys. A **928**, 234 (2014).
- [29] J. Xu, T. Song, C. M. Ko, and F. Li, Phys. Rev. Lett. **112**, 012301 (2014).
- [30] J. Beringer *et al.* [Particle Data Group Collaboration], Phys. Rev. D **86**, 010001 (2012).